Editors' Suggestion

Two-dimensional Weyl half-semimetal and tunable quantum anomalous Hall effect

Jing-Yang You,[1] Cong Chen,[2,3] Zhen Zhang,[1] Xian-Lei Sheng,[2,3,*] Shengyuan A. Yang,[3,4,†] and Gang Su[1,5,‡]

[1]*School of Physical Sciences, University of Chinese Academy of Sciences, Beijing 100049, China*

[2]*Department of Physics, Key Laboratory of Micro-nano Measurement-Manipulation and Physics (Ministry of Education), Beihang University, Beijing 100191, China*

[3]*Research Laboratory for Quantum Materials, Singapore University of Technology and Design, Singapore 487372, Singapore*

[4]*Center for Quantum Transport and Thermal Energy Science, School of Physics and Technology, Nanjing Normal University, Nanjing 210023, China*

[5]*Kavli Institute for Theoretical Sciences and CAS Center for Excellence in Topological Quantum Computation, University of Chinese Academy of Sciences, Beijing 100190, China*

(Received 14 March 2019; revised manuscript received 30 May 2019; published 19 August 2019)

Topological states of matter and two-dimensional (2D) magnetism are two fascinating topics attracting tremendous interest in current research. In this work, we explore their interplay in a single 2D material system by proposing a different topological quantum state of matter—the 2D Weyl half-semimetal (WHS), which features 2D Weyl points at the Fermi level belonging to a single spin channel, such that the low-energy electrons are described by fully spin polarized 2D Weyl fermions. We provide the condition to realize this state, which requires an in-plane magnetization and a preserved vertical mirror symmetry. Remarkably, we prove that the WHS state is a critical state sitting at the topological phase transition between two quantum anomalous Hall (QAH) insulator phases with opposite Chern numbers, such that a switching of the QAH states as well as the direction of chiral edge channels can be readily achieved by rotating the magnetization direction. Furthermore, we predict a concrete 2D material, monolayer $PtCl_3$, as a candidate for realizing the 2D WHS state and the above intriguing effects. Our findings open up a new direction of research at the confluent point of topology and magnetism in two dimensions, and the revealed route towards switchable QAH phases will enable new designs of topological nanoelectronic devices.

DOI: 10.1103/PhysRevB.100.064408

I. INTRODUCTION

As an emerging topological phase of three-dimensional (3D) materials, Weyl semimetals have been attracting extensive attention in recent research [1–9]. In a Weyl semimetal, the conduction and valence bands cross linearly at isolated twofold-degenerate Weyl points in the Brillouin zone (BZ), such that the low-energy electrons resemble the relativistic Weyl fermions; on the surface of a Weyl semimetal, there exist peculiar Fermi arc surface states. The bulk Weyl electrons and the surface Fermi arcs endow Weyl semimetals with many extraordinary properties [10–14], such as ultrahigh mobility [15], negative magnetoresistance [16,17], colossal photovoltaic response [18,19], and enhanced catalytic behavior [20].

Is it possible to extend the concept of Weyl semimetals to two dimensions (2D)? This extension is a nontrivial task. In 3D, a Weyl point is topologically stable: Any perturbation can only displace it but cannot destroy it [9]. However, in 2D, the topological protection is lost due to the reduced dimension, and additional crystal symmetries must be required for stabilizing a Weyl point [5]. Note that the "Dirac" point found in graphene and in some ferromagnetic materials [21–23] is conceptually different from the Weyl point discussed here. The nodal points in those systems are unstable under spin-orbit coupling (SOC) [24], whereas the 2D Weyl point here is robust against SOC. In addition, the nodal point in graphene is fourfold degenerate if spin is counted, whereas a 2D Weyl point is twofold degenerate. So far, a 2D Weyl semimetal has not been reported [25].

A prerequisite for realizing a Weyl semimetal, whether 2D or 3D, is to break either the inversion ($\mathcal{P}$) or the time reversal ($\mathcal{T}$) symmetry because otherwise, each band would be at least twofold spin degenerate, and their crossing point would be at least fourfold degenerate, not of Weyl type. The case with broken $\mathcal{T}$, i.e., a magnetic Weyl semimetal, is especially interesting, as it offers an opportunity to study the fascinating interplay between the magnetic ordering and band topology [1,26–30]. In 2D, the interest further comes from the potential applications in fast-response spintronic nanodevices and is strongly motivated by the recent experimental demonstration of several 2D magnetic materials, such as CrI_3 [31], $Cr_2Ge_2Te_6$ [32], and VSe_2 [33].

In 2D, breaking $\mathcal{T}$ with magnetic ordering is also crucial for another line of research, namely, the exploration of the quantum anomalous Hall (QAH) effect. The QAH effect is realized in a 2D magnetic insulating system. It features dissipationless chiral channels on the edge of the sample, which can be used to make topological transistors with

*xlsheng@buaa.edu.cn
†shengyuan_yang@sutd.edu.sg
‡gsu@ucas.ac.cn

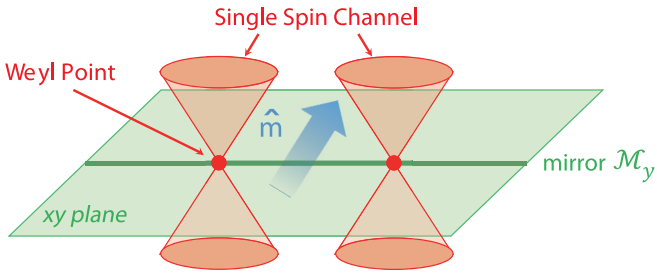

FIG. 1. Schematic figure showing the condition for achieving the two-dimensional Weyl half-semimetal state. Here, the low-energy bands are from a single spin channel. The Weyl points formed at Fermi level are protected by the vertical mirror plane (mirror line) M_y of the 2D system. The magnetization is required to be perpendicular to this mirror plane in order to preserve M_y.

ultralow dissipation and power consumption. So far, the QAH effect has been demonstrated in only a few quantum well systems via magnetic doping [34–41]. The research faces the following challenges. First, the long-range ordering and the uniformity of magnetism are difficult to control in the magnetic doping approach. It is therefore much desired to achieve the QAH effect in a 2D material with intrinsic magnetic ordering. Second, in the existing QAH systems, the switch of the edge channel propagating direction requires the reversal of the magnetization, which typically involves a large applied magnetic field (higher than the coercive field). Hence, to enable practical applications, an alternative switching method must be explored.

Herein, we address *all* above-mentioned challenges by discovering a different state of matter—a 2D Weyl half-semimetal (2D WHS). As indicated by its name, this state is both a Weyl semimetal and a half-metal, with fully spin polarized Weyl points at the Fermi level formed in a single spin channel (see Fig. 1). The low-energy carriers in the state are therefore *fully* spin polarized 2D Weyl fermions. We analyze the condition to realize this state, which requires an in-plane magnetization and a preserved vertical mirror symmetry (i.e., the mirror line in 2D). Remarkably, we show that breaking the mirror will open a gap at the Weyl points and turn the system into a QAH insulator, which can be readily achieved by rotating the in-plane magnetization. More importantly, we prove that the 2D WHS state represents a critical point between two QAH insulator phases with opposite Chern numbers (i.e., with opposite propagating edge channels). Thus, a moderate applied in-plane magnetic field can switch the propagating direction of QAH edge channels. As a concrete example, we show that the 2D WHS state and the above interesting effects can be realized in monolayer $PtCl_3$. Our work addresses both conceptual and practical challenges. It not only reveals a state of matter but also offers promising material platforms for novel topological spintronics applications at nanoscale.

II. CONDITION FOR 2D WHS

Let's start by analyzing the condition needed for realizing a 2D WHS state. To have a half-metal, we need to have ferromagnetic ordering, which in most cases is achieved by incorporating transition-metal elements with partially filled d or f shells. By definition, a Weyl point is a twofold-degenerate nodal point formed by linear crossing between two bands. To stabilize the Weyl point in 2D, we need a symmetry to decouple the two crossing bands; namely, if the two bands have different symmetry eigenvalues, then their crossing point will be protected. Note that the added ferromagnetic ordering typically destroys many symmetries of the underlying crystal lattice but leaves a possible mirror perpendicular to the magnetization intact; that is, if the crystal lattice has a mirror and if the magnetization direction is normal to the mirror, then the mirror will still be preserved in the ferromagnetic state (because the magnetization is a pseudovector). It follows that two bands can linearly cross to form a Weyl point if they have opposite mirror eigenvalues.

In the following, we discuss two possible cases depending on the orientation of the magnetization vector $\hat{\boldsymbol{m}}$.

Case 1. If $\hat{\boldsymbol{m}}$ is perpendicular to the 2D material layer, i.e., in the z direction, then a horizonal mirror plane may be preserved (if the crystal lattice has such a symmetry). However, since the *whole* 2D BZ is invariant under the mirror plane, the generic band crossing for this case would be a Weyl loop rather than a Weyl point. Such a magnetic Weyl loop in 2D was recently proposed by Wang *et al.* [42] and identified in monolayer MnN.

Case 2. If $\hat{\boldsymbol{m}}$ is in the 2D material plane, then a mirror line in the plane may be preserved. In this case, a Weyl point can be stabilized on the mirror-invariant path in the BZ. This case is schematically illustrated in Fig. 1.

This analysis shows that a ferromagnetic 2D material having a magnetic ground state corresponding to case 2 may realize a 2D WHS. In addition, we note that a single Weyl point in the BZ is forbidden by the no-go theorem [43]. There must be at least a pair of Weyl points (see Fig. 1). To have both Weyl points pinned at the Fermi level, they need to be connected by a certain symmetry operation (which is not $\mathcal{T}$ since it is already broken). For example, the two Weyl points can be connected by $\mathcal{P}$ if inversion is preserved for the system. Another point to note is that to have the Weyl points fully exposed at the Fermi level (without other extraneous bands), it is preferred to have low-energy bands with higher dispersion and hence larger band widths. Thus, the d elements would be a better choice than the f elements.

To summarize, in searching for 2D WHS materials, we require the system to satisfy the following conditions: (1) The 2D material must contain transition-metal elements and have a ferromagnetic ground state. (2) In the ground state, the magnetization direction must be in plane and preserves a mirror line. (3) It is desired to have two bands close to the Fermi level which have opposite mirror eigenvalues on the mirror-invariant path. (4) Besides the mirror line, another symmetry must exist that can connect the pair of Weyl points on the mirror-invariant path.

III. MATERIAL EXAMPLE

We reveal a concrete example of 2D WHS, monolayer $PtCl_3$, which is illustrated in Fig. 2(a). It consists of a Pt atomic layer sandwiched by two Cl atomic layers, where the

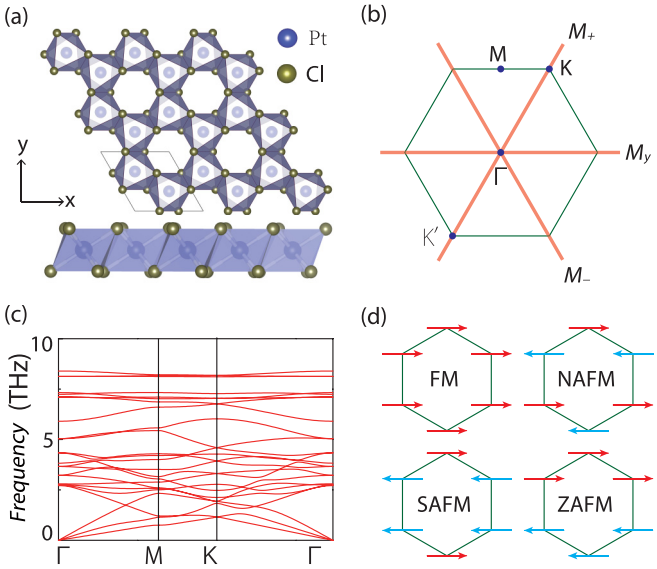

FIG. 2. (a) Top and side views of monolayer $PtCl_3$, with the edge-sharing $PtCl_6$ octahedron forming a honeycomb lattice. (b) First Brillouin zone for monolayer $PtCl_3$ with high-symmetry points labeled. We also mark the orientation of the three vertical mirror planes for the lattice structure (red lines). (c) Phonon spectrum for monolayer $PtCl_3$. (d) Possible magnetic configurations considered: ferromagnet (FM), Néel antiferromagnet (NAFM), stripe AFM (SAFM), and zigzag AFM (ZAFM). The magnetic moments are on the Pt sites forming a honeycomb lattice.

Pt atoms form a honeycomb lattice and each Pt is surrounded by six Cl atoms forming an octahedral crystal field. It takes the same structure as monolayer CrI_3 [31] and $RuCl_3$ [44], which have been experimentally shown to be 2D magnetic materials. The lattice has point group symmetry D_{3d}, with generators of a rotoreflection S_6 and a vertical mirror M_y. Combining these two operations leads to another two mirrors, as illustrated in Fig. 2(b), and also inversion $\mathcal{P}$. The optimized lattice constant from our first-principles calculations is 6.428 Å. (The calculation details are presented in the Appendix.) To confirm its stability, we calculate the phonon spectrum, which shows no imaginary frequency mode [see Fig. 2(c)], indicating that monolayer $PtCl_3$ is dynamically stable. Moreover, we have performed a first-principles swarm structural search and found that the structure in Fig. 2(a) is the global minimum for 2D $PtCl_3$ [45].

Here, Pt is a $5d$ transition-metal element with a partially filled d shell, which may provide the magnetism needed. Indeed, our calculations show that monolayer $PtCl_3$ favors a ferromagnetic (FM) ground state over the antiferromagnetic (AFM) or the paramagnetic (PM) states [see Fig. 2(d) and Table I]. Furthermore, the FM state is found to be a half-metal, i.e., with a single spin channel present at the Fermi level, as can be observed from the projected density of states (DOS) in Fig. 3(b) and the band structure in Fig. 3(c).

To understand this, we note that under the octahedral crystal field, Pt $5d$ orbitals are split into t_{2g} and e_g groups, with the latter being energetically higher. For Pt^{3+} with seven valence electrons, Pt t_{2g} orbitals will be fully filled. Since the crystal field in $PtCl_3$ is stronger than the exchange field,

TABLE I. The total energy $E_{\rm tot}$ per unit cell (in meV, relative to $E_{\rm tot}$ of the FM^y ground state) as well as spin $\langle S\rangle$ and orbital $\langle O\rangle$ moments (in units of μ_B) for several magnetic configurations calculated by the generalized gradient approximation + SOC + U method. The superscript in each configuration indicates the magnetic polarization direction.

	FM^y	$NAFM^y$	$SAFM^y$	$ZAFM^y$	FM^z	FM^x	PM
$E_{\rm tot}$	0.00	316.61	233.84	96.19	5.29	0.67	331.07
$\langle S\rangle$	0.76	0.80	0.78	0.77	0.76	0.76	0
$\langle O\rangle$	0.19	0.23	0.20	0.20	0.25	0.19	0

the fully filled t_{2g} orbitals are away from the Fermi level. On the other hand, Pt e_g orbitals are filled by one electron and hence are fully spin polarized. Because there are two Pt atoms in the primitive cell, the bands dominated by e_g orbitals are half filled for one spin channel and empty for the other, as schematically depicted in Fig. 3(a). The bands around the Fermi level are completely from the spin-up subband of e_g orbitals, therefore making it a half-metal with 100% spin polarization.

Next, we shall pin down the magnetization direction for the FM ground state. We compare the energies by scanning the magnetization direction $\hat{\boldsymbol{m}}$ (with SOC included), and find that (i) in-plane directions are energetically preferred over the out-of-plane ones and (ii) among the in-plane ones, the directions perpendicular to the vertical mirrors (i.e., the armchair direction for the Pt honeycomb lattice) have the lowest energy (see Table I). Thus, one of the three mirrors (the one

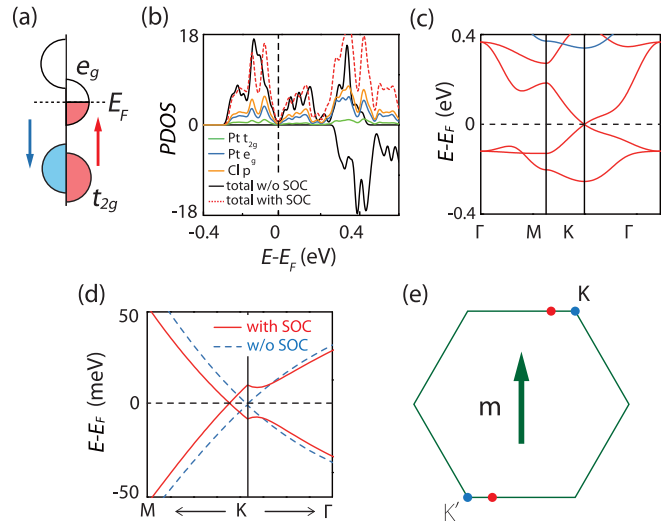

FIG. 3. (a) Schematic depiction of the orbital splitting in monolayer $PtCl_3$. (b) Spin-resolved partial density of states (PDOS) for monolayer $PtCl_3$ projected on different orbitals. (c) Band structure without spin-orbit coupling (SOC). The red and blue bands are for spin-majority (spin-up) and spin-minority (spin-down) channels, respectively. (d) Enlarged view of the band structure around the Weyl point. The red solid (blue dashed) lines are for the bands with (without) SOC. (e) Two Weyl points are located at K/K' points without SOC (blue points), and they are shifted along the x direction on the mirror-invariant line after considering SOC (red points).

perpendicular to $\hat{\boldsymbol{m}}$) is maintained in the FM ground state. The magnetic interaction around the ground-state configuration may be approximately described by the following spin Hamiltonian

$$H = -\sum_{\langle i,j\rangle} J\left(S_i^x S_j^x + S_i^y S_j^y\right) - \sum_i D\left(S_i^y\right)^2, \tag{1}$$

where $S^{x,y}$ is the spin operator, $\langle i, j\rangle$ denotes the summation over nearest neighboring sites, J and D denote the strengths for exchange interaction and anisotropy, respectively. The values of J and D can be extracted from the first-principles calculations. Approximating the model as an anisotropic 2D XY ferromagnet, the Curie temperature for the FM state can be estimated [46–48] as $T_C \approx 200$ K.

Our analysis so far confirms that the magnetic configuration for monolayer $PtCl_3$ satisfies the condition for 2D WHS posed at the beginning. Next, we investigate its electronic band structure. From the band plot in Fig. 3(c), one observes the following remarkable feature: the conduction and valence bands cross linearly at the Fermi level both without and with SOC. Since the two crossing bands are fully spin polarized (spin up), the crossing point is twofold degenerate and represents a 2D Weyl point. Owing to the preserved inversion symmetry, there is a pair of Weyl points in the BZ, sitting on the mirror-invariant path [see the illustration in Fig. 3(e)]. Thus, the ground state for $PtCl_3$ is indeed a 2D WHS, with the low-energy electrons being 100% spin-polarized 2D Weyl fermions.

IV. EFFECTIVE MODEL

To characterize the low-energy band structure for the 2D WHS state, we construct a $k \cdot p$ effective model. In the absence of SOC, the pair of Weyl points is located at the K and K' points of the BZ, similar to graphene, but here they are formed by a single spin species. Without SOC, the spin and the orbital part of the electronic wave function are decoupled, and hence, all crystalline symmetries are preserved for each spin channel separately like for spinless particles. The $k \cdot p$ model $\mathcal{H}_0$ is subjected to the C_{3v} little group at K (K'), with two generators, C_{3z} and M_y. The symmetry constraints are given by

$$C_{3z}\mathcal{H}_0(q_+, q_-)\, C_{3z}^{-1} = \mathcal{H}_0(q_+ e^{i2\pi/3}, q_- e^{-i2\pi/3}), \tag{2}$$

$$M_y \mathcal{H}_0(q_x, q_y) M_y^{-1} = \mathcal{H}_0(q_x, -q_y), \tag{3}$$

where $\boldsymbol{q}$ is measured from K (K') and $q_\pm = q_x \pm i q_y$. And the two Weyl points are related by inversion $\mathcal{P}$. In the basis of the 2D irreducible representation E for C_{3v}, we find that to linear order in q, the effective model takes the form of the 2D Weyl model,

$$\mathcal{H}_0(\boldsymbol{q}) = v_F(\tau q_x \sigma_x + q_y \sigma_y), \tag{4}$$

where v_F is the Fermi velocity, $\tau = \pm$ for the K or K' point, and σ_i are the Pauli matrices acting in the space of the two basis states. Thus, the low-energy electrons indeed resemble 2D Weyl fermions. It is worth noting that despite its similarity to the low-energy model for graphene [49], the model basis and hence the described fermions here for the 2D WHS are fully spin polarized.

The inclusion of SOC pins the ground-state magnetization perpendicular to one of the vertical mirrors (taken to be M_y here). It follows that the C_{3z} symmetry is broken but M_y is still preserved. The preserved M_y dictates that the spin-up and spin-down bands are still fully spin polarized (along y) *without* hybridization by SOC. And the two Weyl points are still protected on M_y, except their locations are slightly shifted from K and K' to some nearby points on the M_y-invariant path K-K', as shown in Fig. 3(e). On the level of the effective model, to leading order in k, SOC introduces the following term:

$$\mathcal{H}_{\rm SOC} = \eta \sigma_x \tag{5}$$

for both K and K' points. As a result, the original Weyl point at K or K' is shifted by $\mp\eta/v_F$ along the x direction (i.e., on the mirror-invariant line) but does not open a gap. This is consistent with our theoretical analysis, and the first-principles calculation result in Fig. 3(d). Thus, we can conclude that the ground state of monolayer $PtCl_3$ indeed realizes a 2D WHS, with a pair of fully spin polarized Weyl points robust under SOC.

V. TUNABLE QAH PHASES

Next, we investigate the transition from 2D WHS to QAH phases. Because the Weyl points in 2D WHS are protected by the mirror M_y, breaking M_y will generally remove the Weyl points and open an energy gap. This symmetry breaking can be easily achieved by slightly rotating $\hat{\boldsymbol{m}}$ away from the ground-state orientation. On the level of the effective model, this effect is represented by adding a mass term, $\mathcal{H}_\Delta = \frac{\Delta}{2}\sigma_z$ (with $|\Delta|$ being the gap size), such that the model becomes

$$\mathcal{H} = \mathcal{H}_0 + \mathcal{H}_{\rm SOC} + \mathcal{H}_\Delta. \tag{6}$$

It is well known that the gap opening at a 2D Weyl point would induce a finite Berry curvature $\Omega(\boldsymbol{q}) = -2\mathrm{Im}\langle\partial_{q_x} u_v|\partial_{q_y} u_v\rangle$, where $|u_v\rangle$ is the eigenstate of the valence band. The integral of Berry curvature in a region around the (original) Weyl point gives a valley topological charge of $\pm 1/2$ [50,51], with the sign determined by $\mathrm{sgn}(\Delta)$. Since $\mathcal{T}$ is broken in the 2D WHS state, the Chern number $\mathcal{C} = \int_{\rm BZ} \Omega(\boldsymbol{k}) d\boldsymbol{k}$, which is the integral of Berry curvature over the BZ, is typically nonzero. Particularly, because Ω is an even function under inversion, when the two Weyl points are connected by $\mathcal{P}$, the two valley topological charges must be identical, and we should have $\mathcal{C} = 1$ or -1. (Note that there may exist a Chern number contribution from deeper valence bands, although the chance is unlikely for real materials.) This analysis demonstrates that breaking the mirror symmetry will transform a 2D WHS into a QAH insulator.

Furthermore, we prove that the 2D WHS state must be a critical point between two QAH phases with opposite Chern numbers. Because the Berry curvature in 2D is an odd function under a vertical mirror, any two QAH phases related by the mirror operation [such as the two in Fig. 5(b) below] must have opposite Chern numbers. Therefore, the WHS state must sit at the critical point of a topological phase transition between two different QAH insulator phases. Since a topological phase transition happens only when the conduction and valence bands touch, this argument in turn

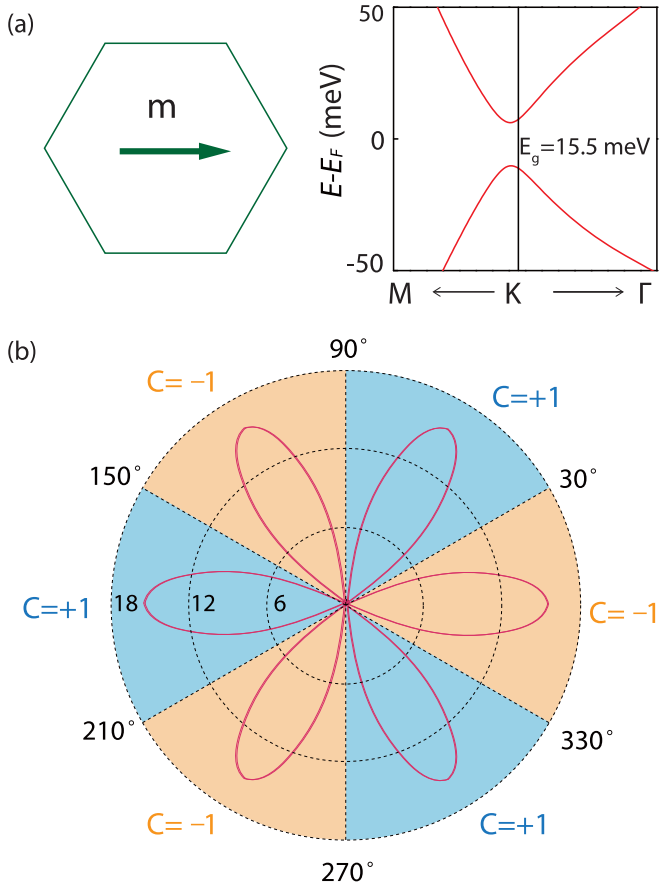

FIG. 4. (a) A gap is opened at the original Weyl point when the magnetization is along the zigzag direction. (b) The flowerlike curve (red line) shows the band gap as a function of the azimuthal angle ϕ for the magnetization direction, where the polar radius indicates the gap value (in meV). Blue (orange) indicates the regions with Chern number $\mathcal{C} = +1$ (-1).

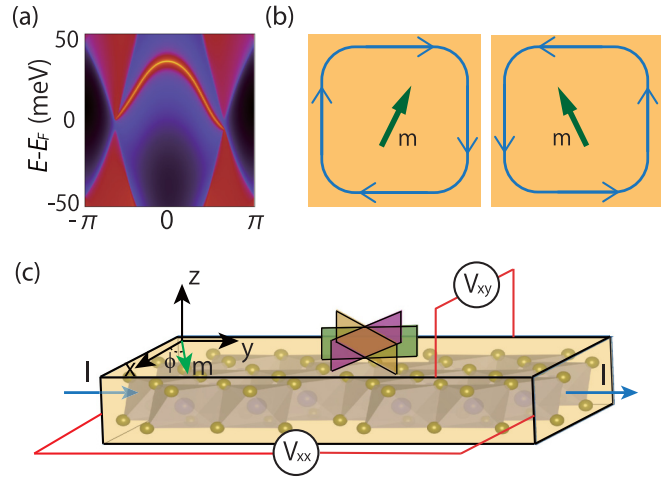

FIG. 5. (a) The edge spectrum corresponding to the case in Fig. 4(a), showing the existence of gapless chiral edge states. (b) Schematic top views of a finite-size sample. By tuning the magnetization direction to regions with opposite Chern numbers, one can switch the propagation direction of the chiral edge channel. This can be probed by the standard transport measurement setup as in (c).

shows that the gap closing and hence the Weyl points in the 2D WHS state are protected.

To verify these conclusions in monolayer $PtCl_3$, in Fig. 4(a), we plot the band structure when the magnetization is along the the $+x$ direction (i.e., the zigzag direction for the Pt honeycomb lattice). Clearly, a finite band gap ~ 15.5 meV is opened at the original Weyl point. By evaluating the Chern number from first-principles calculations, we confirm that this is a QAH insulator with a finite Chern number $\mathcal{C} = -1$. In Fig. 4(b), we plot the band gap and the Chern number as functions of angle ϕ, which is the azimuthal angle for the magnetization vector $\hat{\boldsymbol{m}}$, assuming $\hat{\boldsymbol{m}}$ is rotated in plane. One observes that the gap vanishes at $\phi = \pm\frac{\pi}{6}$, $\pm\frac{\pi}{2}$, and $\pm\frac{5\pi}{6}$, at which one of the three vertical mirrors is preserved, and the state corresponds to a 2D WHS. In regions between these values, the gap becomes nonzero, and the Chern number takes values alternating between $+1$ and -1 for the QAH phases. These observations perfectly agree with our theory.

The hallmark of the QAH phase is the existence of chiral edge states, i.e., gapless channels at the edge propagating unidirectionally. Figure 5(a) shows the edge spectrum for monolayer $PtCl_3$ in the QAH phase in Fig. 4(a) (with $\mathcal{C} = -1$), obtained from first-principles calculations, which confirms the existence of one chiral channel per edge. Because the chirality of the edge channel is determined by the sign of Chern number, the two QAH phases with $\mathcal{C} = \pm 1$ must have edge channels propagating in opposite directions. Consequently, by tuning across the topological phase transition (through the WHS state) between the two QAH phases, one can switch the propagating direction of the edge channel [see Fig. 5(b)]. This can be easily detected with a standard electrical transport measurement, as shown in Fig. 5(c).

VI. DISCUSSION AND CONCLUSION

We have some remarks before closing. First, the proposed 2D WHS here is protected by the mirror symmetry. Hence, it should be robust under biaxial strain or uniaxial strains along the in-plane high-symmetry directions, which preserve the mirror. For more general strains (like shear strain), the 2D WHS state would transform into the QAH phase. Strains can further be used to tune the gap of the QAH state. For example, the band gap for the case in Fig. 4(a) can be increased to $\sim$20 meV under a biaxial 5% compressive strain on monolayer $PtCl_3$.

Second, the electronic correlation effect could be important for transition-metal compounds, although it is typically weak for $5d$ elements like Pt. Here, we test the effect of correlation on monolayer $PtCl_3$ via the density-functional theory $+ U$ approach [52,53]. We find that the results are qualitatively unchanged for U values up to 2 eV, and only for very large U (> 2.8 eV) can the system be transformed into a Mott insulator. Since a typical U value for $5d$ elements is less than 1.5 eV [54,55], the calculation results presented here should be robust.

Third, we have provided conditions for a 2D WHS in Sec. II. However, the search for real material candidates is still a nontrivial task. This is because the magnetic ground state and the low-energy band structure cannot be easily

inferred from the material structure and composition. We have investigated several 2D materials with a CrI_3-type [31] lattice structure, but only $PtCl_3$ turns out to be a 2D WHS in the ground state. For example, we find that monolayer $PtBr_3$ [56] has an out-of-plane magnetization in the ground state, and it is a quantum anomalous Hall insulator. On the other hand, monolayer VCl_3 [23,55], $OsCl_3$ [55], and PtI_3 [56] have in-plane magnetization, but the magnetization is along the x direction, which breaks the mirror line. As a result, the Weyl point is gapped when the SOC is included. In the future, high-throughput computation may be a possible approach to search for 2D topological materials. For the case of 2D WHSs, it should combine an intelligent structural search and magnetic ground-state determination. The symmetry conditions we obtained here could be of great help in facilitating the search process.

In conclusion, we have proposed a topological state of matter in 2D: the 2D WHS. It represents a nontrivial conceptual development that extends the Weyl concept from 3D to 2D. We obtained symmetry conditions to realize this state. We showed that compared to the 3D Weyl semimetals, the loss of topological protection in 2D actually turns out to be an advantage: Gapping out the 2D WHS via symmetry breaking offers a route to achieve the long-sought QAH phase. Furthermore, through coupling magnetism with Weyl band topology, we demonstrated topological phase control by tuning the magnetic ordering. We proved that the 2D WHS represents a critical point at the topological phase transition between two QAH phases with opposite Chern numbers, so that switching the direction of the chiral edge channels requires only a small tuning by an in-plane magnetic field. In practice, such magnetic field is typically much smaller than the field needed to achieve a magnetic reversal. This may offer a new mechanism for designing novel topological electronic devices.

ACKNOWLEDGMENTS

We thank D. L. Deng for helpful discussion. This work is supported in part by the National Key R&D Program of China (Grant No. 2018FYA0305800), the Strategic Priority Research Program of CAS (Grants No. XDB28000000, No. XBD07010100), the NSFC (Grants No. 11834014, No. 14474279, No. 11504013), the Beijing Municipal Science and Technology Commission (Grant No. Z118100004218001), and the Singapore Ministry of Education AcRF Tier 2 (Grant No. MOE2015-T2-2-144).

APPENDIX: FIRST-PRINCIPLES METHOD

Our first-principles calculations were based on density-functional theory (DFT) as implemented in the Vienna Ab initio Simulation Package (VASP) [57,58], using the projector augmented-wave method [59]. The generalized gradient approximation with the Perdew-Burke-Ernzerhof [60] realization was adopted for the exchange-correlation functional. The plane-wave cutoff energy was set to 520 eV. A Monkhorst-Pack k-point mesh [61] with a size of $11 \times 11 \times 1$ was used for the BZ sampling. To account for the correlation effects for transition-metal elements, the DFT $+ U$ method [52,53] was used for calculating the band structures. The crystal structure was optimized until the forces on the ions were less than 0.01 eV/Å. The surface spectrum was calculated by using the Wannier functions and the iterative Green's function method [62–65].

[1] X. Wan, A. M. Turner, A. Vishwanath, and S. Y. Savrasov, Phys. Rev. B **83**, 205101 (2011).
[2] S. Murakami, New J. Phys. **9**, 356 (2007).
[3] A. A. Burkov and L. Balents, Phys. Rev. Lett. **107**, 127205 (2011).
[4] C.-K. Chiu, J. C. Y. Teo, A. P. Schnyder, and S. Ryu, Rev. Mod. Phys. **88**, 035005 (2016).
[5] S. A. Yang, SPIN **06**, 1640003 (2016).
[6] A. A. Burkov, Nat. Mater. **15**, 1145 (2016).
[7] X. Dai, Nat. Phys. **12**, 727 (2016).
[8] A. Bansil, H. Lin, and T. Das, Rev. Mod. Phys. **88**, 021004 (2016).
[9] N. P. Armitage, E. J. Mele, and A. Vishwanath, Rev. Mod. Phys. **90**, 015001 (2018).
[10] Q.-D. Jiang, H. Jiang, H. Liu, Q.-F. Sun, and X. C. Xie, Phys. Rev. Lett. **115**, 156602 (2015).
[11] S. A. Yang, H. Pan, and F. Zhang, Phys. Rev. Lett. **115**, 156603 (2015).
[12] D. T. Son and B. Z. Spivak, Phys. Rev. B **88**, 104412 (2013).
[13] A. A. Burkov, Phys. Rev. B **91**, 245157 (2015).
[14] S. Guan, Z.-M. Yu, Y. Liu, G.-B. Liu, L. Dong, Y. Lu, Y. Yao, and S. A. Yang, npj Quantum Mater. **2**, 23 (2017).
[15] C. Shekhar, A. K. Nayak, Y. Sun, M. Schmidt, M. Nicklas, I. Leermakers, U. Zeitler, Y. Skourski, J. Wosnitza, Z. Liu, Y. Chen, W. Schnelle, H. Borrmann, Y. Grin, C. Felser, and B. Yan, Nat. Phys. **11**, 645 (2015).
[16] X. Huang, L. Zhao, Y. Long, P. Wang, D. Chen, Z. Yang, H. Liang, M. Xue, H. Weng, Z. Fang, X. Dai, and G. Chen, Phys. Rev. X **5**, 031023 (2015).
[17] Y. Wang, E. Liu, H. Liu, Y. Pan, L. Zhang, J. Zeng, Y. Fu, M. Wang, K. Xu, Z. Huang, Z. Wang, H.-Z. Lu, D. Xing, B. Wang, X. Wan, and F. Miao, Nat. Commun. **7**, 13142 (2016).
[18] G. B. Osterhoudt, L. K. Diebel, M. J. Gray, X. Yang, J. Stanco, X. Huang, B. Shen, N. Ni, P. J. W. Moll, Y. Ran, and K. S. Burch, Nat. Mater. **18**, 471 (2019).
[19] J. Ma, Q. Gu, Y. Liu, J. Lai, P. Yu, X. Zhuo, Z. Liu, J.-H. Chen, J. Feng, and D. Sun, Nat. Mater. **18**, 476 (2019).
[20] C. R. Rajamathi, U. Gupta, N. Kumar, H. Yang, Y. Sun, V. Süß, C. Shekhar, M. Schmidt, H. Blumtritt, P. Werner, B. Yan, S. Parkin, C. Felser, and C. N. R. Rao, Adv. Mater. **29**, 1606202 (2017).
[21] H. Ishizuka and Y. Motome, Phys. Rev. Lett. **109**, 237207 (2012).
[22] Y. Li, D. West, H. Huang, J. Li, S. B. Zhang, and W. Duan, Phys. Rev. B **92**, 201403(R) (2015).
[23] J. He, S. Ma, P. Lyu, and P. Nachtigall, J. Mater. Chem. C **4**, 2518 (2016).
[24] C. L. Kane and E. J. Mele, Phys. Rev. Lett. **95**, 226801 (2005).

[25] A stable 2D Weyl point was recently reported in monolayer GaTeI [W. Wu, Y. Jiao, S. Li, X.-L. Sheng, Z.-M. Yu, and S. A. Yang, Phys. Rev. Mater. **3**, 054203 (2019)], although the system is not a semimetal.
[26] G. Xu, H. Weng, Z. Wang, X. Dai, and Z. Fang, Phys. Rev. Lett. **107**, 186806 (2011).
[27] Z. Wang, M. G. Vergniory, S. Kushwaha, M. Hirschberger, E. V. Chulkov, A. Ernst, N. P. Ong, R. J. Cava, and B. A. Bernevig, Phys. Rev. Lett. **117**, 236401 (2016).
[28] J. Kübler and C. Felser, Europhys. Lett. **114**, 47005 (2016).
[29] Q. Xu, E. Liu, W. Shi, L. Muechler, J. Gayles, C. Felser, and Y. Sun, Phys. Rev. B **97**, 235416 (2018).
[30] C. Chen, Z.-M. Yu, S. Li, Z. Chen, X.-L. Sheng, and S. A. Yang, Phys. Rev. B **99**, 075131 (2019).
[31] B. Huang, G. Clark, E. Navarro-Moratalla, D. R. Klein, R. Cheng, K. L. Seyler, D. Zhong, E. Schmidgall, M. A. McGuire, D. H. Cobden, W. Yao, D. Xiao, P. Jarillo-Herrero, and X. Xu, Nature (London) **546**, 270 (2017).
[32] C. Gong, L. Li, Z. Li, H. Ji, A. Stern, Y. Xia, T. Cao, W. Bao, C. Wang, Y. Wang, Z. Q. Qiu, R. J. Cava, S. G. Louie, J. Xia, and X. Zhang, Nature (London) **546**, 265 (2017).
[33] M. Bonilla, S. Kolekar, Y. Ma, H. C. Diaz, V. Kalappattil, R. Das, T. Eggers, H. R. Gutierrez, M.-H. Phan, and M. Batzill, Nat. Nanotechnol. **13**, 289 (2018).
[34] C.-Z. Chang, J. Zhang, X. Feng, J. Shen, Z. Zhang, M. Guo, K. Li, Y. Ou, P. Wei, L.-L. Wang, Z.-Q. Ji, Y. Feng, S. Ji, X. Chen, J. Jia, X. Dai, Z. Fang, S.-C. Zhang, K. He, Y. Wang, L. Lu, X.-C. Ma, and Q.-K. Xue, Science **340**, 167 (2013).
[35] J. G. Checkelsky, R. Yoshimi, A. Tsukazaki, K. S. Takahashi, Y. Kozuka, J. Falson, M. Kawasaki, and Y. Tokura, Nat. Phys. **10**, 731 (2014).
[36] X. Kou, S.-T. Guo, Y. Fan, L. Pan, M. Lang, Y. Jiang, Q. Shao, T. Nie, K. Murata, J. Tang, Y. Wang, L. He, T.-K. Lee, W.-L. Lee, and K. L. Wang, Phys. Rev. Lett. **113**, 137201 (2014).
[37] A. J. Bestwick, E. J. Fox, X. Kou, L. Pan, K. L. Wang, and D. Goldhaber-Gordon, Phys. Rev. Lett. **114**, 187201 (2015).
[38] X. Kou, L. Pan, J. Wang, Y. Fan, E. S. Choi, W.-L. Lee, T. Nie, K. Murata, Q. Shao, S.-C. Zhang, and K. L. Wang, Nat. Commun. **6**, 8474 (2015).
[39] A. Kandala, A. Richardella, S. Kempinger, C.-X. Liu, and N. Samarth, Nat. Commun. **6**, 7434 (2015).
[40] Y. Feng, X. Feng, Y. Ou, J. Wang, C. Liu, L. Zhang, D. Zhao, G. Jiang, S.-C. Zhang, K. He, X. Ma, Q.-K. Xue, and Y. Wang, Phys. Rev. Lett. **115**, 126801 (2015).
[41] C.-Z. Chang, W. Zhao, J. Li, J. K. Jain, C. Liu, J. S. Moodera, and M. H. W. Chan, Phys. Rev. Lett. **117**, 126802 (2016).
[42] S.-S. Wang, Z.-M. Yu, Y. Liu, Y. Jiao, S. Guan, X.-L. Sheng, and S. A. Yang, Phys. Rev. Mater. **3**, 084201 (2019).
[43] H. Nielsen and M. Ninomiya, Phys. Lett. B **130**, 389 (1983).
[44] A. Banerjee, C. A. Bridges, J. Q. Yan, A. A. Aczel, L. Li, M. B. Stone, G. E. Granroth, M. D. Lumsden, Y. Yiu, J. Knolle, S. Bhattacharjee, D. L. Kovrizhin, R. Moessner, D. A. Tennant, D. G. Mandrus, and S. E. Nagler, Nat. Mater. **15**, 733 (2016).
[45] Y. Jiao, X.-L. Sheng, and S. A. Yang (unpublished).
[46] D. Spirin and Y. Fridman, Phys. B (Amsterdam, Neth.) **325**, 410 (2003).
[47] B. V. Costa, A. R. Pereira, and A. S. T. Pires, Phys. Rev. B **54**, 3019 (1996).
[48] Y.-q. Ma and W. Figueiredo, Phys. Rev. B **55**, 5604 (1997).
[49] A. H. Castro Neto, F. Guinea, N. M. R. Peres, K. S. Novoselov, and A. K. Geim, Rev. Mod. Phys. **81**, 109 (2009).
[50] W. Yao, S. A. Yang, and Q. Niu, Phys. Rev. Lett. **102**, 096801 (2009).
[51] H. Pan, X. Li, F. Zhang, and S. A. Yang, Phys. Rev. B **92**, 041404(R) (2015).
[52] V. I. Anisimov, J. Zaanen, and O. K. Andersen, Phys. Rev. B **44**, 943 (1991).
[53] S. L. Dudarev, G. A. Botton, S. Y. Savrasov, C. J. Humphreys, and A. P. Sutton, Phys. Rev. B **57**, 1505 (1998).
[54] X. Wan, A. Vishwanath, and S. Y. Savrasov, Phys. Rev. Lett. **108**, 146601 (2012).
[55] X.-L. Sheng and B. K. Nikolić, Phys. Rev. B **95**, 201402(R) (2017).
[56] J.-Y. You, Z. Zhang, B. Gu, and G. Su, arXiv:1904.11357.
[57] G. Kresse and J. Hafner, Phys. Rev. B **49**, 14251 (1994).
[58] G. Kresse and J. Furthmüller, Phys. Rev. B **54**, 11169 (1996).
[59] P. E. Blöchl, Phys. Rev. B **50**, 17953 (1994).
[60] J. P. Perdew, K. Burke, and M. Ernzerhof, Phys. Rev. Lett. **77**, 3865 (1996).
[61] H. J. Monkhorst and J. D. Pack, Phys. Rev. B **13**, 5188 (1976).
[62] N. Marzari and D. Vanderbilt, Phys. Rev. B **56**, 12847 (1997).
[63] I. Souza, N. Marzari, and D. Vanderbilt, Phys. Rev. B **65**, 035109 (2001).
[64] Q. Wu, S. Zhang, H.-F. Song, M. Troyer, and A. A. Soluyanov, Comput. Phys. Commun. **224**, 405 (2018).
[65] M. P. López Sancho, J. M. López Sancho, and J. Rubio, J. Phys. F **14**, 1205 (1984); **15**, 851 (1985).